This MICCAI paper is the Open Access version, provided by the MICCAI Society. It is identical to the accepted version, except for the format and this watermark; the final published version is available on SpringerLink.

Mesenteric Arterial Vessel Segmentation in Abdominal CT with Small Bowel Obstruction

Hyuna Cho, Tejas S. Mathai, Ronald M. Summers

National Institutes of Health (NIH) Clinical Center, Bethesda, MD 20892, USA
{hyuna.cho, tejas.mathai}@nih.gov, rsummers@cc.nih.gov

Abstract. Segmentation of mesenteric arteries in abdominal CT is important for characterizing the anatomical relationship between the mesenteric vasculature and the small bowel, yet it remains challenging due to their small caliber, complex branching patterns, proximity to veins, and limited availability of annotated data. In this work, we introduce a three-step semi-automatic pipeline for constructing mesenteric arterial vessel masks on 3D abdominal CT scans, spanning from the superior mesenteric artery to distal branches near the small bowel. Our method combines iterative-learning-based preliminary mask generation, anatomy-guided distal vessel generation, and topology-aware post-processing. Using the generated annotations as labels, we evaluate existing state-of-the-art segmentation models on the Dice score and establish a standard for mesenteric arterial vessel segmentation. Our proposed annotation pipeline provides a foundation for automatic vessel segmentation and topology-aware analysis of small-bowel diseases in abdominal CT.

Keywords: Vessel Segmentation · Small Bowel Obstruction · Abdominal CT

1 Introduction

The small bowel is a highly deformable organ whose loop configuration varies substantially across patients, scans, and disease states. This variability makes it difficult to establish stable anatomical correspondence based on bowel morphology alone. In contrast, the mesenteric arterial tree provides a patient-specific anatomical reference that is rooted at the superior mesenteric artery (SMA) and extends through the mesentery toward the small bowel wall [3, 16]. Since distal mesenteric arterial branches supply specific, fixed regions of the small bowel, identifying vessels extending toward the small bowel provides useful spatial anchors for localizing bowel segments, characterizing their vascular supply, tracking bowel path, and preoperative planning in abdominal surgery [6, 23, 24].

Such vessel–bowel relationships are particularly useful for understanding small bowel obstruction (SBO), where bowel loops are dilated, displaced, or distorted [14]. In SBO, accurate localization of obstructed bowel loops and transition zones is important for evaluating disease severity and identifying complications related to vascular compromise, including strangulation, ischemia, and necrosis [2, 11].

In this setting, explicit delineation of the mesenteric arterial tree provides complementary anatomical information for SBO assessment since the arterial tree serves as a patient-specific spatial reference for localizing bowel segments.

Several public vessel datasets, such as MSD Hepatic Vessel [1] and Aortic Vessel Tree [12], have supported the development of vascular segmentation methods in CT. Moreover, large-scale multi-organ CT segmentation datasets [9, 19] also include some major vessels, such as the aorta and iliac artery. However, they focus on specific vascular beds and major abdominal vessels, without dense annotations of distal mesenteric arterial branches extending toward the small bowel. Moreover, generating voxel-level annotations of such distal branches is time-consuming and challenging because they are small, tortuous, and frequently exhibit weak or heterogeneous contrast enhancement, requiring approximately 6 hours of manual effort per CT scan. This difficulty is further compounded by the proximity and similarity between the SMA-derived arterial branches and the superior mesenteric vein (SMV)-derived venous branches.

In this work, we propose a framework to generate segmentation labels for the mesenteric arteries (ranging from the SMA to distal vessels extending toward the small bowel) and use them to train state-of-the-art segmentation models. The pipeline consists of three steps: (1) preliminary anatomical mask generation, (2) distal vessel generation, and (3) topology-aware post-processing. First, masks of the SMA and SMV trunks with proximal branches were obtained using an iterative learning strategy. A small number of manually annotated cases were used to train an nnU-Net [7], and the model predictions were iteratively corrected and added back to the training set. In parallel, a small-bowel mask was obtained using TotalSegmentator [19] to provide anatomical information for post-processing. Second, distal vessel candidates were selected using contrast- and vesselness-based filtering, and artery–vein distance constraints. Finally, topology-aware post-processing was applied to reconnect plausible fragmented distal branches, remove intra-bowel false positives, and retain a single SMA-rooted arterial tree. The resulting masks were used to train segmentation models on 3D SBO CT scans so that distal mesenteric arterial branches are automatically segmented in unseen scans without requiring time-consuming manual annotation.

2 Method

2.1 Dataset

We used an internal HIPAA-compliant 3D contrast-enhanced abdominal CT dataset collected from patients with SBO. Each scan covers the entire small bowel, including the duodenum, jejunum, and ileum. The CT images were reconstructed using a soft-tissue kernel with a slice thickness of 2mm and a reconstruction interval of 1mm. Voxel values are expressed in Hounsfield units (HU), and blood vessels are highlighted using an intravenous contrast agent (ISOVUE).

The dataset consists of 117 CT studies obtained from 101 subjects. Among the 101 subjects, 87 subjects have a single study, while 14 subjects have longitudinal studies. Specifically, 12 subjects have two studies, and 2 subjects have

Table 1: Characteristics of the Small Bowel Obstruction dataset.

# Subjects	# Studies	Phase (PV / Art.)	Sex (M / F)	Age (Mean ± Std)	Manufacturer (Siemens / Toshiba)
101	117	109 / 8	59 / 42	55.1 ± 14.5	115 / 2

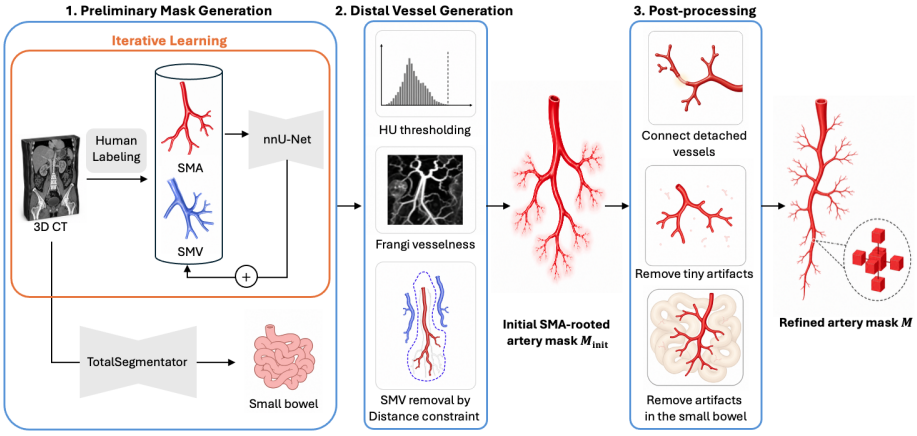

Fig. 1: Overview of the proposed pipeline for mesenteric artery mask generation. Given a contrast-enhanced abdominal CT scan, SMA and SMV seed masks are generated using an iterative learning, and a small-bowel mask is obtained for anatomical guidance. Distal vessel candidates are selected using contrast- and vesselness-based thresholding with SMA/SMV distance constraints. After post-processing, a single connected arterial tree is constructed. The vessel, small bowel, and CT icons were made by using ChatGPT v5.5 [10].

three studies. Among the 117 scans, 109 were acquired in the portal venous (PV) phase, and the remaining 8 scans were acquired in the arterial phase. Demographic and imaging characteristics of the dataset are summarized in Table 1.

2.2 Preliminary Mask Generation

Given a CT scan, we construct preliminary masks for the SMA and SMV trunks with proximal vessels, and the small bowel, which serve as seeds and constraints for distal arterial vessel extraction. The SMA mask serves as the arterial seed for subsequent artery growing, while the SMV mask is used as a venous constraint to suppress leakage into venous structures. Since both arteries and veins are tubular structures and are in close, the SMV mask provides an important anatomical prior to prevent false-positive arterial segmentation.

As generating the SMA and SMV labels for 1 CT volume can take ∼3 hours, an iterative learning strategy was employed to reduce the need for cumbersome manual annotation. A subset of CT scans is first manually annotated for the

SMA and SMV by an expert grader using ITK-SNAP [22], under the supervision of a senior board-certified radiologist with over 30 years of experience. These annotations are used to train a 3D nnU-Net [7], which is then applied to unlabeled scans to generate preliminary predictions. The predicted masks are visually inspected and corrected when necessary, and the corrected cases are added back to the training set for the next iteration. This iterative process progressively improves the quality of the SMA and SMV masks.

In parallel, a small-bowel mask is obtained using TotalSegmentator [19] to provide anatomical context for post-processing, where false positives within the small bowel interior are removed while preserving vessels adjacent to the bowel wall. The resulting SMA, SMV, and small-bowel masks are used as inputs for the proposed distal arterial vessel generation pipeline.

2.3 Distal Arterial Vessel Generation from SMA

Given the CT image and preliminary masks, the second stage generates distal arterial vessel candidates extending from the SMA. All operations are performed within a cropped region of interest (ROI), defined by the bounding box of the union of the SMA and SMV masks with an additional 95-voxel margin. This ROI-based processing reduces memory usage and prevents the algorithm from growing into distant abdominal structures, such as the colon.

HU Thresholding. Since the vessels are enhanced by a contrast agent, we first select voxels with intensity values within a predefined HU range. Let $I(x)$ denote the CT intensity at voxel x. The HU-based candidate mask is defined as

$$C_{\mathrm{HU}} = \{x \mid h_{\min} \leq I(x) \leq h_{\max}\},$$

where $h_{\min} = 95$ and $h_{\max} = 370$ are lower and upper thresholds, respectively. This step removes low-intensity background regions and high-intensity nonvascular structures (e.g., bones) that do not correspond to contrast-enhanced vessels.

Frangi Vesselness Filtering. HU thresholding alone is insufficient because abdominal organs and bowel-wall structures have similar intensity values to enhanced vessels. Therefore, we further apply a 3D Frangi vesselness filter [4] to enhance tubular structures. The Frangi response $F(I)(x)$ is computed at multiple scales to identify diverse thicknesses of vessels, and voxels with vesselness values above a threshold $\tau = 0.0012$ are retained:

$$C_{\mathrm{Frangi}} = \{x \mid F(I)(x) \geq \tau\}.$$

The core vessel candidate mask is obtained by combining the HU and vesselness constraints as $C_{\mathrm{core}} = C_{\mathrm{HU}} \cap C_{\mathrm{Frangi}}$. This step favors thin, elongated, vessel-like structures and suppresses non-tubular regions.

Venous Constraints. To distinguish the SMA-derived arterial tree from nearby veins, we impose venous constraints using the SMV mask. First, the SMV mask is dilated with a spherical structuring element by 3 voxels to form a safety margin around venous structures as C_{vein}. Candidate voxels inside this region are removed, except for voxels belonging to the SMA seed. Second, we define an

artery-territory constraint based on the relative distance to the SMA and SMV. Let $d_{\mathrm{SMA}}(x)$ and $d_{\mathrm{SMV}}(x)$ denote the Euclidean distance from voxel x to the SMA and SMV masks, respectively. We define an arterial territory mask as

$$C_{\mathrm{dist}} = \{x \mid d_{\mathrm{SMA}}(x) < \alpha d_{\mathrm{SMV}}(x)\},$$

where $\alpha = 2.0$ controls the allowed spatial extent of the arterial territory. For example, a larger α allows a broader arterial territory to be considered for vessel candidates. The vessel candidate mask is then defined as

$$C = C_{\mathrm{core}} \cap C_{\mathrm{dist}} \cap \overline{C_{\mathrm{vein}}},$$

which defines the search space for artery growing. Starting from the SMA seed, region growing is performed within C to obtain the initial SMA-rooted arterial mask M_{init}. The growing process is repeated until no additional voxels are added or a maximum number of iterations is reached. This initial tree contains the SMA seed and distal arterial branches under the defined vessel and venous constraints.

2.4 Post-processing for Arterial Vessel Mask Generation

The M_{init} may still contain small fragmented distal branches, and false positives inside the small bowel. Thus, we apply post-processing to improve the anatomical plausibility and topological consistency of the generated artery mask.

First, we recover fragmented distal branches by bridging plausible local gaps within anatomically constrained candidate regions. To identify branch termini, the M_{init} is converted into a one-voxel-thick skeleton, and endpoints are defined as voxels with a single neighboring skeleton voxel. Nearby endpoint pairs are connected if their outward directions are mutually aligned and the cost of local paths is low. For each endpoint p_i, the outward branch direction $\mathbf{v}_i$ is estimated as the principal eigenvector of the covariance matrix of neighboring skeleton voxels. For two endpoints p_i and p_j, a gap direction from p_i to p_j is defined as:

$$\mathbf{g}_{ij} = \frac{p_j - p_i}{\|p_j - p_i\|}.$$

The pair is connectable if the two outward directions are mutually aligned:

$$\mathbf{v}_i^\top \mathbf{g}_{ij} \geq \epsilon \quad \text{and} \quad \mathbf{v}_j^\top (-\mathbf{g}_{ij}) \geq \epsilon,$$

where $-1 \leq \epsilon \leq 1$ controls the degree of alignment between the two directions.

A low-cost path is then searched within the constrained candidate region, where core vessel candidates are assigned lower costs than relaxed growth candidates. High-cost paths are rejected, and a relaxed HU range is allowed only near M_{init} with venous and bowel-interior exclusion. This step recovers distal arterial vessels disconnected due to weak contrast enhancement or partial volume effects.

Subsequently, the remaining small, isolated components and intra-bowel false positives are removed. As a result, a single continuous arterial tree originating from the SMA is obtained, where neighboring voxels are connected by sharing a face in 3D space. The resulting binary mask M is used as the ground-truth label for supervised vessel segmentation. We visually inspected 50 randomly selected generated masks overlaid on the corresponding CT images to assess label quality.

Table 2: (Left) Experimental results of iterative learning for SMA and SMV mask generation. (Right) Model performance comparison for vessel segmentation.

# Scans	Dice (%)
6	54.1
8	53.5
11	68.6
14	71.5
18	73.9
33	82.0

Model	Model type	Dice (%)	Precision (%)	Recall (%)
nnU-Net [7]	CNN	**56.5 ± 1.9**	**69.7 ± 3.2**	53.5 ± 3.2
MedNeXt [15]	CNN	50.1 ± 2.7	54.6 ± 3.2	52.8 ± 3.2
EfficientMedNeXt [13]	CNN	46.8 ± 3.7	51.8 ± 4.8	51.0 ± 5.9
3D-GCCN [8]	CNN + GNN	40.9 ± 4.2	37.5 ± 3.7	**56.6 ± 3.4**
Swin-UNETR [5]	Transformer	37.9 ± 3.1	32.8 ± 2.6	47.5 ± 5.3
Diff-UNet [21]	Diffusion model	34.0 ± 4.1	31.5 ± 5.6	45.0 ± 6.1

3 Experimental Setup

Semi-automatic vessel mask construction. We set the HU-based vessel candidate range as $h_{\min} = 95$ and $h_{\max} = 370$, and the Frangi vesselness threshold as $\tau = 0.0012$. The Frangi response was computed at multiple scales to capture vessels with different diameters. For the SMA–SMV distance-based constraint, we used $\alpha = 2.0$, allowing candidate voxels to be included when they were closer to the SMA seed than to the SMV up to this relative distance factor. During endpoint-based gap bridging, the ϵ was set to 0, allowing endpoint directions within 90° of the inter-endpoint direction.

Supervised vessel segmentation. We compare six recent 3D medical image segmentation models across diverse architectural families, including CNN-based models, nnU-Net (3D full-res) [7], MedNeXt [15], and EfficientMedNeXt [13]; a hybrid CNN–GNN model, 3D-GCCN [8]; a transformer-based model, Swin-UNETR [5]; and a diffusion-based model, Diff-UNet [21]. All models are trained using 5-fold cross-validation under the same train and validation splits.

Iterative learning strategy. To reduce the manual annotation burden for the SMA and SMV masks, we used an iterative learning strategy. Starting from 6 manually annotated CT scans, an nnU-Net model was trained to jointly segment the SMA and SMV. The predictions were manually corrected when necessary and added back to the training set. This process was repeated 5 times to progressively expand the annotated dataset and improve the quality of preliminary masks.

4 Result

4.1 Results of Iterative Learning

Table 2 summarizes the iterative learning process with the number of manually annotated cases and the corresponding Dice score. As the number of annotated cases increased from 6 to 33, the validation Dice score improved from 54.1% to 82.0%, demonstrating that iterative correction and retraining substantially improved the quality of preliminary SMA and SMV masks.

4.2 Comparison of the Vessel Segmentation Performance

Table 2 compares the 5-fold cross-validation performance of 3D segmentation models on the SBO dataset by using M as ground truth. Overall, CNN-based

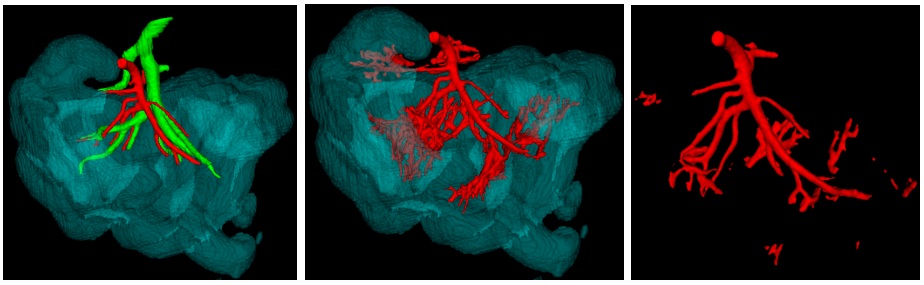

(a) Preliminary masks (b) Artery mask M with small bowel (c) Prediction of nnU-Net

Fig. 2: (a) Preliminary masks of small bowel (blue), SMA (red), and SMV (green) with proximal vessels. (b) Artery mask M constructed by our method with the small bowel. The whole structure is fully connected, and distal branches are in contact with the small bowel wall. (c) Artery segmentation result of nnU-Net.

models outperformed transformer-, diffusion-, and graph-based models. Specifically, nnU-Net achieved the best performance with a Dice score of 56.5%. MedNeXt obtained the second-best result with a Dice score of 50.1%, followed by EfficientMedNeXt with 46.8%. Also, a CNN–GNN hybrid model, 3D-GCCN, obtained a Dice score of 40.9%. Compared with these CNN-based models, Swin-UNETR and Diff-UNet showed lower performance with a Dice score of 37.9% and 34.0%, respectively. For statistical comparison, we also performed a two-sided paired Wilcoxon signed-rank test [20] between the two best-performing models, nnU-Net and MedNeXt, using per-case Dice scores. As a result, nnU-Net significantly outperformed MedNeXt (median Dice, 58.3 vs. 51.5; p=$2.8e^{-9}$).

4.3 Qualitative Evaluation of Artery Masks

For qualitative evaluation, we show 3D visualizations of the preliminary anatomical masks, the artery mask M generated by our proposed pipeline, and the segmentation result of nnU-Net in Fig. 2. Specifically, Fig. 2(a) visualizes the preliminary anatomical masks, including the small bowel, SMA, and SMV trunks with proximal vessels. The SMA and SMV masks provide the arterial seed and venous constraint for the proposed vessel generation pipeline, while the small-bowel mask provides anatomical context for post-processing.

Fig. 2(b) shows the artery mask M constructed by our method together with the small-bowel mask. The generated arterial tree extends from the proximal SMA to multiple distal branches near the small bowel wall. Compared with the SMA seed in Fig. 2(a), the proposed pipeline recovers a substantial number of distal branches while maintaining a connected SMA-rooted tree structure. The generated distal vessels contact the small bowel wall, preserving the anatomical relationship between the mesenteric arteries and the small bowel.

Fig. 2(c) shows the result of nnU-Net on the 5-fold CV segmentation task. Although the main arterial trunk and several large branches are detected, many

distal branches remain fragmented or missing, and small isolated false positives are observed. This result highlights the difficulty of automatically segmenting small mesenteric arterial branches from 3D abdominal CT, especially for thin vessels with weak contrast enhancement and complex branching patterns.

5 Discussion

Findings. In this work, we proposed a semi-automatic pipeline for mesenteric arterial vessel mask generation in small bowel obstruction CT. Using the SMA as the arterial root and the SMV and small bowel masks as anatomical constraints, the pipeline constructs arterial masks extending from the proximal SMA to distal branches near the small bowel. This approach reduces the burden of fully manual annotation and enables scalable construction of anatomically plausible vessel masks. We further evaluated six 3D segmentation models across four different architectural families using the constructed artery masks as ground truths. Among them, nnU-Net performed the best, and CNN models outperformed other architectures. This suggests that local convolutional features and multi-scale spatial aggregation remain effective for segmenting small vessels, which have sparse foreground regions with thin and complex branching patterns. Nevertheless, the relatively modest Dice scores across all models indicate that automatic segmentation of distal mesenteric arteries remains challenging, especially due to weak contrast enhancement, small vessel caliber, and similarity to nearby venous structures.
Limitations. The quality of the artery masks depends on the accuracy of preliminary masks, as they affect distal branch generation and post-processing steps. Moreover, since the current pipeline was developed for contrast-enhanced CT scans from patients with small bowel obstruction, further validation is needed to evaluate its generalizability to other datasets and acquisition protocols.
Prospects of Application. The generated mesenteric artery masks are particularly useful for downstream analysis of vessel–bowel relationships, including bowel segment localization and small bowel path tracking. For example, existing small bowel path tracking methods [17,18] largely rely on bowel morphology and wall detection, which can be unreliable when bowel loops are dilated, collapsed, displaced, or closely apposed in SBO. However, distal mesenteric arteries provide complementary extraluminal anatomical landmarks for resolving ambiguous bowel trajectories in distorted anatomy. By adding vascular context to existing bowel tracking approaches, the proposed method may support more robust path tracking and image-based assessment of small-bowel disease. From a broader perspective, this framework has the potential to be adapted to other vascular structures with thin and complex branches, such as hepatic, renal, or pulmonary vessels, where fully manual annotation remains challenging.

Disclosure of Interests. Dr. Ronald M. Summers received royalties for patents or software licenses from iCAD, Philips, ScanMed, PingAn, TranslationHoldings, and MGB. The remaining authors have no relevant financial or non-financial interests to disclose.

Acknowledgments. This work was supported by the Intramural Research Program of the NIH Clinical Center (project number 1Z01 CL040004). The research used the high-performance computing facilities of the NIH Biowulf cluster. The authors would like to thank the NIH Biomedical Translational Research Information System (BTRIS) for their support.

Disclaimer. This research was supported in part by the Intramural Research Program of the National Institutes of Health (NIH). The contributions of the NIH authors are considered Works of the United States Government. The findings and conclusions presented in this paper are those of the authors and do not necessarily reflect the views of the NIH or the U.S. Department of Health and Human Services.

References

1. Antonelli, M., et al.: The medical segmentation decathlon. Nature Communications (2022). https://doi.org/10.1038/s41467-022-30695-9
2. Diamond, M., Lee, J., LeBedis, C.A.: Small bowel obstruction and ischemia. Radiologic Clinics **57**(4), 689–703 (2019)
3. Erden, A., Cumhur, T., Ölçer, T.: Superior mesenteric artery blood flow in patients with small bowel diseases: evaluation with duplex doppler sonography. Journal of clinical ultrasound **26**(1), 37–41 (1998)
4. Frangi, A.F., et al.: Multiscale vessel enhancement filtering. In: International conference on medical image computing and computer-assisted intervention. pp. 130–137. Springer (1998)
5. Hatamizadeh, A., et al.: Swin unetr: Swin transformers for semantic segmentation of brain tumors in mri images. In: International MICCAI brainlesion workshop. pp. 272–284. Springer (2021)
6. Horton, K.M., Fishman, E.K.: Volume-rendered 3d ct of the mesenteric vasculature: normal anatomy, anatomic variants, and pathologic conditions. Radiographics **22**(1), 161–172 (2002)
7. Isensee, F., et al.: nnu-net: a self-configuring method for deep learning-based biomedical image segmentation. Nature methods **18**(2), 203–211 (2021)
8. Li, R., et al.: 3d graph-connectivity constrained network for hepatic vessel segmentation. IEEE Journal of Biomedical and Health Informatics **26**(3), 1251–1262 (2021)
9. Li, W., et al.: Abdomenatlas: A large-scale, detailed-annotated, & multi-center dataset for efficient transfer learning and open algorithmic benchmarking. Medical Image Analysis p. 103285 (2024), https://github.com/MrGiovanni/AbdomenAtlas
10. OpenAI: Chatgpt (2026), https://chat.openai.com, large language model. Generated June 15, 2026
11. Paulson, E.K., Thompson, W.M.: Review of small-bowel obstruction: the diagnosis and when to worry. Radiology **275**(2), 332–342 (2015)
12. Radl, L., et al.: Avt: Multicenter aortic vessel tree cta dataset collection with ground truth segmentation masks. Data in brief **40**, 107801 (2022)
13. Rahman, M.M., Munir, M., Marculescu, R.: Efficientmednext: Multi-receptive dilated convolutions for medical image segmentation. In: International Conference on Medical Image Computing and Computer-Assisted Intervention. pp. 196–206. Springer (2025)

14. Rami Reddy, S.R., Cappell, M.S.: A systematic review of the clinical presentation, diagnosis, and treatment of small bowel obstruction. Current gastroenterology reports **19**(6), 28 (2017)
15. Roy, S., et al.: Mednext: transformer-driven scaling of convnets for medical image segmentation. In: International conference on medical image computing and computer-assisted intervention. pp. 405–415. Springer (2023)
16. Shaikh, H., Wehrle, C.J., Khorasani-Zadeh, A.: Anatomy, abdomen and pelvis: superior mesenteric artery. In: StatPearls [Internet]. StatPearls Publishing (2023)
17. Shin, S.Y., Lee, S., Summers, R.M.: Graph-based small bowel path tracking with cylindrical constraints. In: 2022 IEEE 19th International Symposium on Biomedical Imaging (ISBI). pp. 1–5. IEEE (2022)
18. Shin, S.Y., Lee, S., Summers, R.M.: A graph-theoretic algorithm for small bowel path tracking in ct scans. In: Medical Imaging 2022: Computer-Aided Diagnosis. vol. 12033, pp. 863–868. SPIE (2022)
19. Wasserthal, J., et al.: Totalsegmentator: robust segmentation of 104 anatomic structures in ct images. Radiology: Artificial Intelligence **5**(5), e230024 (2023)
20. Wilcoxon, F.: Individual comparisons by ranking methods. In: Breakthroughs in statistics: Methodology and distribution, pp. 196–202. Springer (1992)
21. Xing, Z., et al.: Diff-unet: A diffusion embedded network for robust 3d medical image segmentation. Medical Image Analysis **105**, 103654 (2025)
22. Yushkevich, P.A., Gao, Y., Gerig, G.: Itk-snap: An interactive tool for semi-automatic segmentation of multi-modality biomedical images. In: 2016 38th annual international conference of the IEEE engineering in medicine and biology society (EMBC). pp. 3342–3345. IEEE (2016)
23. Zhang, W., et al.: Automatic anatomical labeling of abdominal arteries for small bowel evaluation on 3d ct scans. In: 2013 IEEE 10th international symposium on biomedical imaging. pp. 210–213. IEEE (2013)
24. Zhang, W., et al.: Mesenteric vasculature-guided small bowel segmentation on 3-d ct. IEEE transactions on medical imaging **32**(11), 2006–2021 (2013)